Structural basis for the extended CAP-Gly domains of p150^{glued} binding to microtubules and the implication for tubulin dynamics

Qianmin Wang[a], Alvaro H. Crevenna[b], Ines Kunze[a], and Naoko Mizuno[a,1]

[a]Cellular and Membrane Trafficking, Max Planck Institute of Biochemistry, D-82152 Martinsried, Germany; and [b]Physical Chemistry, Department for Chemistry and Biochemistry and Center for NanoScience, Ludwig-Maximilians-Universität München, D-81377 Munich, Germany

Edited* by Donald Caspar, Institute of Molecular Biophysics, Cataumet, MA, and approved June 26, 2014 (received for review February 20, 2014)

p150^{glued} belongs to a group of proteins accumulating at microtubule plus ends (+TIPs). It plays a key role in initiating retrograde transport by recruiting and tethering endosomes and dynein to microtubules. p150^{glued} contains an N-terminal microtubule-binding cytoskeleton-associated protein glycine-rich (CAP-Gly) domain that accelerates tubulin polymerization. Although this copolymerization is well-studied using light microscopic techniques, structural consequences of this interaction are elusive. Here, using electron-microscopic and spectroscopic approaches, we provide a detailed structural view of p150^{glued} CAP-Gly binding to microtubules and tubulin. Cryo-EM 3D reconstructions of p150^{glued}-CAP-Gly complexed with microtubules revealed the recognition of the microtubule surface, including tubulin C-terminal tails by CAP-Gly. These binding surfaces differ from other retrograde initiation proteins like EB1 or dynein, which could facilitate the simultaneous attachment of all accessory components. Furthermore, the CAP-Gly domain, with its basic extensions, facilitates lateral and longitudinal interactions of tubulin molecules by covering the tubulin acidic tails. This shielding effect of CAP-Gly and its basic extensions may provide a molecular basis of the roles of p150^{glued} in microtubule dynamics.

dynamic instability | dynactin | cytoskeleton | electron microscopy

The great variety of microtubule-associated proteins and the complexity of their interactions (1) are beginning to rival that of the actin-associated proteins. This complexity reflects the many different roles that actin and microtubules play in cellular cytoskeletal organization and activity. Our study focuses on the structural interactions of tubulin/microtubules with protein fragments corresponding to N-terminal portions of the p150^{glued} subunit of the megadalton dynactin complex. Of particular interest is the 80-amino acid cytoskeleton-associated protein glycine-rich (CAP-Gly) domain (p150^{glued} residues 25–105), which, when harboring critical mutations in neuronal dynactin, leads to devastating neurological disorders (2).

Several studies have characterized the interactions of p150^{glued} with various +end-binding proteins (+TIPs), including end-binding protein 1 (EB1) and CLIP-170 (3–5), and the role of the negatively charged, C-terminal tubulin tails in binding positively charged domains of these proteins to the tubulin surface (6–9). Biophysical observations showed the ability of the +TIPs to promote microtubule polymerization (5, 6, 10). Recently, Lazarus et al. (11) have demonstrated that the N-terminal dimeric portion of p150^{glued} is a neuron-specific anticatastrophe factor acting at the microtubule +end; a mutation in the CAP-Gly domain, which causes the lethal Perry syndrome, when introduced in their recombinant dimeric construct, abolishes the protective anticatastrophic depolymerization activity.

Here, by focusing on a single CAP-Gly domain of p150^{glued}, intrinsic interactions with tubulin and microtubules were identified. The basic p150 fragments cause the lateral association of microtubules by neutralizing their repulsive negative surface charge. By limiting the extent of bundling, cryo-electron microscopic (cryo-EM) 3D reconstructions were obtained for CAP-Gly plus basic extensions connected to the negatively charged, flexible tails of tubulin. These reconstructions indicated a flexible connection of the CAP-Gly domain. Furthermore, this domain facilitated the assembly of tubulins into longitudinally connected oligomers at low temperatures and initiation of polymerization, likely through activating lateral associations of tubulin. The lateral interaction is likely due to the masking of the acidic charge of the tubulin surface. These two observed interactions provide a basis for the microtubule recovery following catastrophes. The properties of the +TIPs are much more than the sum of their parts. However, the identification of intrinsic properties of the components builds a foundation for exploring their cooperative interactions.

Results

EM Observation Shows That the Microtubule Lateral Association Is Induced by p150^{glued}. To understand the interaction between p150^{glued} and microtubules in a structural context, we observed the p150^{glued}–microtubule complex using cryo-EM. We generated several p150^{glued} fragments containing the microtubule-binding CAP-Gly domain: namely, the CAP-Gly core [p150(25–105)]; 25 additional N-terminal residues [p150(1–105)]; 40 additional, unstructured C-terminal residues [p150(25–144)]; and both N- and C-terminal extensions [p150(1–144)] (Fig. S1) (12, 13). Both extensions contain several basic residues with predicted pI values of 12.0 and 12.6, respectively, as opposed to rather mild basic pI of 8.9 for CAP-Gly. A microtubule-pelleting assay showed that the binding of CAP-Gly alone to microtubules appears to be fairly weak (Fig. S1*B*, marked with an *), but addition of the upstream/downstream basic patches increased the binding affinity. Quantitative pelleting assays showed that CAP-Gly can recognize both alpha and beta tubulin at saturating levels (Fig. S2*A*). In the presence of 2 μM microtubules with 20 μM p150^{glued}

Significance

This study presents a direct visualization of the microtubule-p150glued(CAP-Gly) complex by cryo-EM and seeks to describe the molecular mechanism of the control of tubulin dynamics by p150 CAP-Gly. It highlights the neutralization of the acidic tubulin surface by the basic extensions of CAP-Gly, resulting in the activation of tubulin polymerization. In the condition where the lateral association is impeded (i.e., at low temperature), the extended CAP-Gly domain induces tubulin dimers to connect longitudinally. The two directional modes of self-association of tubulin suggest a foundation for its dynamic behavior at the tip of microtubules and its regulation.

Author contributions: A.H.C. and N.M. designed research; Q.W., A.H.C., I.K., and N.M. performed research; Q.W., A.H.C., and N.M. analyzed data; and A.H.C. and N.M. wrote the paper.

The authors declare no conflict of interest.

*This Direct Submission article had a prearranged editor.

Freely available online through the PNAS open access option.

Data deposition: The data reported in this paper have been deposited in the Electron Microscopy Data Bank (accession nos. 2673, 2674, and 2675).

[1]To whom correspondence should be addressed. Email: mizuno@biochem.mpg.de.

This article contains supporting information online at www.pnas.org/lookup/suppl/doi:10.1073/pnas.1403135111/-/DCSupplemental.

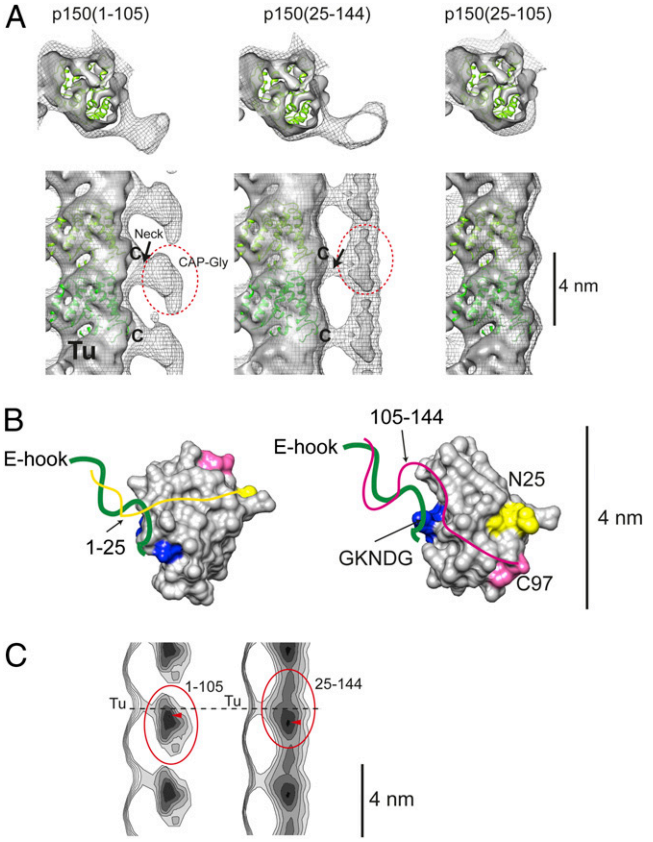

Fig. 1. (*A*) Shown are 3D reconstructions of microtubules with p150(1–105) (*Left*), p150(25–144) (*Center*), and p150(25–105) (*Right*). The sample was prepared by mixing 20-μM protein fragments with 2-μM microtubules in 80 mM Pipes-Na (pH 6.8), 1 mM $MgCl_2$, and 1 mM EGTA. Chicken-wire densities show the reconstructions without amplifying the high-resolution density whereas the amplitude-corrected reconstruction is presented as a solid density, resulting in weakening the density of the decoration. A fitted tubulin atomic model is shown in green (PDB ID code 1TUB). Tubulin E-hooks are missing from the atomic model. The last visible residue from the atomic model is labeled "C." Tu, tubulin protofilament. (*B*) Schematics of the interaction between E-hook and $p150^{glued}$ CAP-Gly. The N- and C-terminal parts of the atomic model of CAP-Gly (PDB ID code 1TXQ) are marked in yellow (N25) and pink (C97), respectively. The N- and C-terminal extensions of the CAP-Gly core are depicted as yellow and pink lines, respectively. These extensions are predicted to be disordered, but the experiments confirm the interactions with tubulin E-hooks (green line). The GKNDG motif interacting with tyrosine at the C terminus of the alpha tubulin E-hook is colored in blue. The mean orientations of the flexibly connected p150(1–105) (*Left*) and p150(25–144) in the reconstructions in *A* are suggested. (*C*) Lateral projection of one protofilament decorated with p150(1–105) (*Left*) and p150(25–144) (*Right*). Circles, CAP-Gly core; arrowheads, the highest density (CAP-Gly core). The dashed line indicates the position of the neck.

fragments, saturation of the proteins on microtubules was achieved, except for p150(25–105) (*SI Discussion* and Figs. S1*B* and S2).

The corresponding complexes observed under cryo-EM showed that microtubules associate with each other to form a lateral assembly (Fig. S1*C*). This assembly was not observed for p150(25–105). These microtubules sometimes opened up showing a sheet-like structure. We selected p150(25–105), p150(1–105), and p150(25–144) for further analysis because they yielded complexes in which microtubules were separated enough for image processing. In contrast, p150(1–144) caused strong microtubule bundling, which hampered structure analysis.

Cryo-EM Reconstruction Shows a Neck Formation of Tubulin E-Hooks and the CAP-Gly Basic Patch. The reconstruction of microtubules bound to the CAP-Gly core p150(25–105) showed nondetectable protein decoration (Fig. 1*A*, *Right*) reflecting the weak interaction. p150(1–105) and p150(25–144) gave enough density to visualize the spatial relation of the CAP-Gly domains bound to the microtubules (Fig. 1*A*, *Left* and *Center*). The CAP-Gly density is located ∼2 nm away from the microtubule surface, connected through a neck protruding out from the microtubule surface. The reconstruction of p150(1–105) (chicken wire displayed density) gave an interpretable density corresponding to the CAP-Gly core, which has comparable size to the crystal structure of the CAP-Gly (PDB ID code 1TXQ) (Fig. 1*B*). We chose not to fit the crystal structure to the reconstruction due to the flexibility of the CAP-Gly binding.

There is no apparent interaction between the core of the microtubules and the CAP-Gly. By adjusting the amplitude of relatively high frequency signals (*SI Materials and Methods*), the microtubule density started revealing secondary structure elements (Fig. 1*A*, gray solid density), which made it feasible to fit the atomic structure of a tubulin dimer. The molecular fitting showed that the C terminus of tubulin is connected to the neck (Fig. 1*A*, labeled with "C"). The ∼15 aa, negatively charged C-terminal tubulin tail (termed the E-hook) was not resolved in the atomic model (PDB ID code 1TUB) because of its flexible nature (14). Judging from the connection of the E-hook containing neck and the tubulin monomer, E-hook is leaning toward the minus end of the microtubule in the p150(1–105)-microtubule reconstruction. As the CAP-Gly core itself attaches to the neck, the neck density should also consist of the mass of the CAP-Gly basic extensions. Proteolytic treatment of the tubulin E-hooks by subtilisin abolished the binding of the CAP-Gly fragments (Fig. S2), also confirming the exclusive binding of the CAP-Gly fragments to E-hooks. On the other hand, the reconstruction of p150(25–144)-microtubule showed a decoration connected along the microtubule axis although the general flat bean-like shapes of CAP-Gly were recognizable by changing the density threshold (Fig. 1*A*, *Center* and 1*C*, *Right*). This density is connected through the neck, indicating that the essential interaction happens through the E-hook.

Based on the pelleting assay (Fig. S1*B*), the binding of the p150 fragments to the microtubules was greatly increased upon the addition of the basic patches (amino acids 1–25 and 106–144). Therefore, the densities connecting CAP-Gly and tubulin core (Fig. 1*A*, neck) likely correspond to E-hooks and the 1–25 basic patch for p150(1–105), and E-hooks and the 106–144 basic patch for p150(25–144) (Table 1). This observation indicates that the binding of CAP-Gly–containing fragments depends on oppositely charged surface interactions rather than a set of specific/conserved interactions. Moreover, the binding affinity of the CAP-Gly core to the tyrosinated E-hook was 11 μM whereas virtually no detectable binding was observed for the detyrosinated E-hook (>130 μM) (Table 1). This increase of the affinity agrees with previous reports (7) showing the recognition of the CAP-Gly core GKNDG motif by tyrosine at the end of the alpha E-hook. It suggests that the GKNDG motif is interacting with the C terminus of tubulin whereas the basic patches 1–25 and 106–144 wrap around the rest of the E-hook to secure the binding (Fig. 1*B*).

Table 1. Dissociation constants (K_d, μM) of $p150^{glued}$ fragments to E-hook peptides using fluorescence correlation spectroscopy

p150 fragments	αY	αE	βC
1–210 dimer	0.8 ± 0.3	3 ± 1	0.8 ± 0.3
1–105	6 ± 3	35 ± 20	9 ± 5
25–105	11 ± 5	> 130	46 ± 20
25–144	5.4 ± 1.5	28 ± 30	10 ± 4
1–144	7 ± 3	13 ± 4	7 ± 2

αY, tyrosinated alpha tubulin E-hook; αE, detyrosinated alpha tubulin E-hook, βC; beta tubulin E-hook.

p150^{glued} CAP-Gly Fragments Flexibly Recognize the Microtubule Surface. The computational amplitude adjustment of the reconstruction weakened the density of the CAP-Gly to a close-to-noise level. This faint density suggests either that the occupancy of the protein fragments is low or that their attachment to the microtubule surface is very flexible. However, the pelleting assay in the corresponding conditions showed the saturation of p150 fragments on the microtubules, supporting a possibility that the blurred density is due to the flexible binding of the p150 fragments.

To explore this aspect in detail, density contours of the reconstructions were calculated. The lateral projections of the reconstructions from radius ~130–180 Å (Fig. 1*C*) showed the strongest density of the p150(1–105) decoration to be 4 Å lower than the neck position (Fig. 1*C*, *Left*, red arrowhead), shifted toward the minus end, but 8 Å for p150(25–144) (Fig. 1*C*, *Right*, red arrowhead). This position corresponds to the core of CAP-Gly, and it suggests a flexible binding mode for the interaction of CAP-Gly fragments with E-hooks. Comparing the overall shapes of the CAP-Gly core densities raises the possibility that the orientation of the CAP-Gly may be flipped between p150(1–105) and p150(25–144) reconstructions (direction shown in Fig. 1*B*).

Further, the recognition site of CAP-Gly was mapped onto microtubules (Fig. 2, blue) and compared with the ones of dynein (Fig. 2*A*, yellow) (15) as well as the yeast EB protein Mal3 (Fig. 2*A*, pink) (16), a binding partner of p150^{glued} during endosomal recruitment. Interestingly, all binding surfaces differ from each other, and there is enough space for all proteins to bind simultaneously to the same microtubule unit. p150^{glued} binds to tubulin where the C-terminal E-hook is located (Fig. 2*A*, marked "C" in red) at the "neck" of the reconstruction. This position is well-separated from the binding sites for dynein/kinesin or EBs. The pelleting assay of the p150(1–144), EB1 CH domain and kinesin head to the microtubule also showed that they all bind to the microtubule surface (Fig. 2*B*, rightmost lane).

Microtubule Lateral Association Is Caused by Shielding of E-Hooks. The saturated decoration of p150^{glued} fragments on the microtubule surface caused microtubules to laterally associate with each other, which made the structural analysis particularly challenging. However, this observation drew our interest and led us to investigate the cause of the bundling triggered by CAP-Gly fragments.

We hypothesized that the lateral association of the microtubules may occur by the fact that CAP-Gly fragments cover the E-hooks. The negatively charged, flexible E-hooks could serve as an electrostatic shield that repels a close approach of neighboring microtubules. Binding of the positively charged p150^{glued} segments to the negatively charged tubulin E-hooks may collapse the mobile barrier that keeps the microtubules apart. To test this hypothesis, we measured the change of turbidity at 400 nm by adding several p150^{glued} fragments to taxol-stabilized microtubules (Fig. S3). The scattering increased as highly positively charged protein fragments were added, from 0.29 for microtubules alone up to 1.7 for p150(1–144) (net charge, +12.7). The degree of the increase in scattering correlates with the lateral association of microtubules observed in the corresponding electron micrographs (Fig. S1*C*). The turbidity was not increased for p150(25–105) (net charge, +1.6), which does not contain any basic patches. Interestingly, the addition of the construct p150 (106–144), which has a net charge of +7 but does not contain CAP-Gly, also caused an increase of turbidity to 0.76 and the bundling of the microtubules. Consistent with this finding, we also observed the increase of turbidity and the lateral association of microtubules when tubulin E-hooks were removed by subtilisin (Fig. S3*B*). Further, we tested the change of turbidity with a control protein that has a high basic charge but is not derived from p150^{glued}. For this purpose, we used histone H2A (15 kDa, net charge, +12.6) as a test case and measured the turbidity changing to 0.81, an increase similar to p150(106–144).

These results altogether suggest that the E-hooks of tubulin form a negative shield on the microtubule surface. The neutralization of the charge by basic proteins repels the shielding and leads to the lateral association of microtubules. The degree of the turbidity increase generally correlates well with the net charge of added protein fragments. This phenomenon does not require any specific protein interaction with microtubules as shown for the case of histone H2A or p150(106–144).

Longitudinal Tubulin Oligomerization Is Induced by CAP-Gly Plus Basic Patch at Low Temperatures. The masking of the acidic tails of tubulin by CAP-Gly plus basic patches causes the lateral association of tubulin. Moreover, previous reports established the ability of p150 fragments to promote the polymerization of microtubules (5, 11). Therefore, we sought to correlate polymerization activity with the charge effects of various CAP-Gly fragments. First, the light scattering of tubulin below the critical concentration for spontaneous polymerization (2 μM) was monitored during a temperature shift from 4 °C to 37 °C (Fig. S4*A*, Tu). Consistent with previous reports, light scattering was elevated: i.e., tubulin polymerization, in the presence of the dimerized CAP-Gly, with its basic extensions [p150(1–210) dimer] (Fig. S4*A*) (11). We also observed assisted tubulin polymerization with p150(1–144) fragments (Fig. S4*B*) although the effect was much less, compared with the dimerized CAP-Gly. The stepwise change of ionic strength in the assay buffer confirmed the sensitivity of the process to the salt concentration,

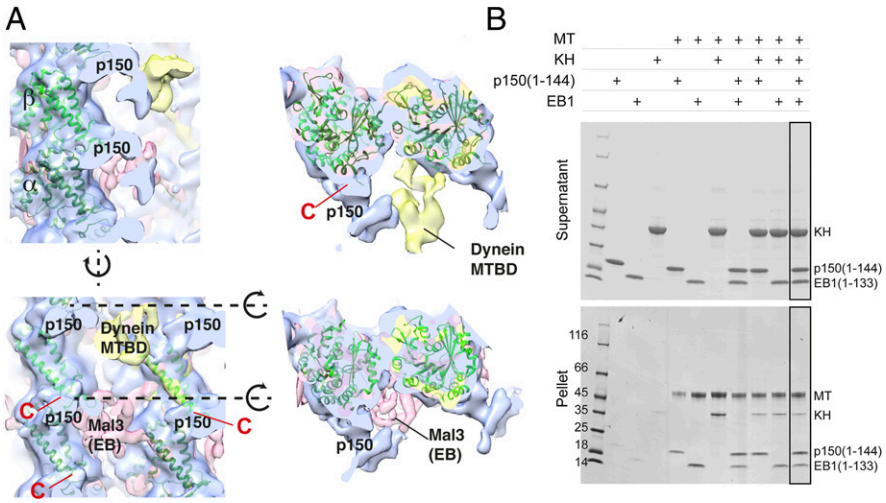

Fig. 2. (*A*) Comparison of the binding surfaces on tubulins for p150^{glued} neck, dynein (MTBD), and Mal3 (EB). The recognition sites of these proteins differ from each other. Red C, the C-terminal end of the tubulin atomic model, which precedes the flexible 15–16 residue E-hooks. Cross-sections of the surface of the side view (dotted line) are shown *Right*. (*B*) Pelleting assay of p150(1–144), kinesin head (KH), EB1 CH domain, and GTPgamaS-stabilized microtubules. The 2-μM microtubules and 20-μM proteins were mixed. Added proteins are indicated as "+." The three proteins bind to microtubules simultaneously.

as expected from the electrostatic binding properties of the proteins. The pronounced tubulin copolymerization with p150 (1–144) was observed when the tubulin concentration was high enough to self-promote polymerization (10 μM) (Fig. S4*C*, red lines).

To connect the tested protein fragments in the context of tubulin polymerization, we used the latter experimental condition to further examine the behavior of tubulins. The light-scattering profiles revealed an elevation of scattering with CAP-Gly, which included the C terminus basic extensions [p150(1–144), p150(25–144)] (Fig. S4*C*, red and purple) whereas the fragments without the extension [p150(1–105), p150(25–105)] did not have a significant influence. Interestingly, the profiles also showed that the presence of the C-terminal extension alone (residues 106–144) increased the final saturation level, agreeing with the increase of the turbidity seen with already polymerized, taxol-stabilized microtubules (Fig. S4*C*, pink). We further detected a striking increase in scattering for tubulin-CAP-Gly mixtures at the stage before the initiation of polymerization at 4 °C (Fig. S5*A*).

To visualize this rise, we analyzed the reaction mixtures using electron microscopy. The protein fragments were confirmed to bind to unpolymerized tubulins (Fig. S5*B*) and the CAP-Gly fragments containing the basic patches 1–25 or 106–144 induced tubulins to form linear, curved oligomers (Fig. 3) with a radius of curvature of ∼17 nm. These oligomers have the same morphology as the separated, curled protofilaments observed in vitro (17).

This similarity indicates that the interaction of the CAP-Gly fragments to tubulin dimers at 4 °C increases tubulin's longitudinal self-affinity.

The degree of oligomerization increased when more positively charged residues were present (Fig. 3 and Fig. S5*C*). When tubulin oligomer formation was induced by the p150(1–210) dimer, which has the most prominent effect on tubulin polymerization (Fig. S4*A*) (11), large agglomerates of tubulin oligomers were visible in EM (Fig. 3). Therefore, it is not feasible to quantify the degree of oligomerization using EM, even though light-scattering experiments showed comparable values with p150(1–144)-induced oligomers (Fig. S5*A*). In contrast, the longitudinal tubulin association did not occur in the presence of only CAP-Gly core, p150(25–105), or the basic patch without CAP-Gly, p150(106–144). These observations suggest that the activation of the longitudinal assembly of tubulin is facilitated by the bridging of both CAP-Gly and the basic extension, possibly like the way shown in the reconstruction of p150(25–144) (Fig. 1*A*, *Center*).

In comparison, CLIP-170 is a member of +TIPs that contains tandem-connected CAP-Gly domains. It has been reported that a CLIP-170 fragment containing only one CAP-Gly (CLIP-170S) does not enhance the polymerization of tubulin whereas a variant containing both CAP-Gly domains (CLIP-170L) increases the polymerization rate (18, 19). We extended this analysis to test whether oligomerization would occur with a CLIP-170-tubulin mixture using EM (Fig. 3). We detected that CLIP-170L induces tubulin oligomerization strongly whereas there was only sporadic oligomer formation with CLIP-170S. These results are consistent with the indication that the observed oligomers have a direct effect on microtubule polymerization.

Tubulin Oligomers Function as Intermediates During Polymerization. To understand the copolymerization of longitudinally connected tubulin oligomers induced by CAP-Gly fragments, we followed the process by dynamic light scattering (DLS). Although tubulin control showed a population of <10 nm (Fig. 4*A*, *Top*, red), the mixture of tubulin with p150(1–144) exhibited the population only at a size distribution of ∼100–1,000 nm (Fig. 4*A*, *Top*, green) at 4 °C. When tubulin polymerization was initiated by a temperature shift to 37 °C, a growing population of an ∼1,000–10,000 nm species was observed after 60–90 s (Fig. 4*A*, 90 s, blue arrow). At the same time, the population of the 100–1,000 nm decreased. After 150 s, the size distribution became comparable with microtubules alone (Fig. 4*A*, *Top*, blue). During this polymerization, the signal of tubulin dimers (1–10 nm) was not detected,

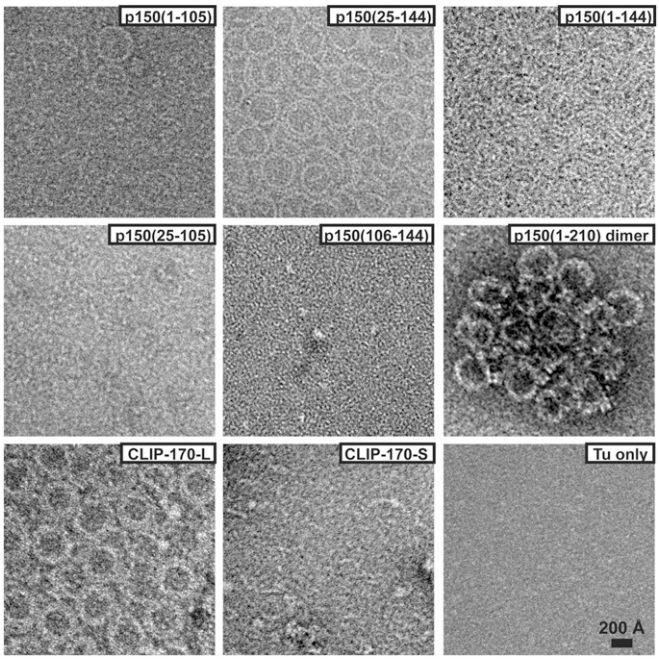

Fig. 3. Negative stain EM observation of tubulin oligomers (10 μM) induced by $p150^{glued}$ fragments (10 μM) at 4 °C. Oligomer formation happens with p150(1–144) and p150(25–144), but there is very little or no oligomerization for p150(1–105), p150(25–105), and p150(106–144). p150(1–210) dimer causes tubulin oligomers and further clustering of the oligomers. CLIP-170L with two tandem CAP-Gly shows similar oligomer formation whereas CLIP-170S with one CAP-Gly shows no oligomeric formation.

strongly indicating that the oligomeric formation of tubulin and p150(1–144) directly transitions to tubulin polymers without disassembling into dimer units.

Further, snapshots of the copolymerization at 300 s were taken by cryo-EM and epifluorescence light microscopy. Consistent with the observations by dynamic light scattering, we could readily detect formations of microtubules. The striking population of laterally connected, sheet-like tubulin polymers was observed as well (Fig. 4*C*, marked as "S" and Fig. S6). The lateral interaction is promoted upon the temperature change to 37 °C. The ends of the closed microtubules often showed a flared morphology, sometimes with fragments of straightened oligomers attached to each other (Fig. S6, guided in magenta). The corresponding experiment using light microscopy revealed a strong colocalization of p150(1–144) at the end of microtubules as well as a weak colocalization on the surface of growing microtubules (Fig. 4*B*, arrows).

Taken together, the preformed, longitudinally connected tubulin oligomers (before tubulin polymerization) activate their lateral interactions upon temperature change, resulting in sheet-like formations. The oligomers tend to cluster at the end of the closed growing microtubule, likely incorporating into the microtubule structure.

GTP Hydrolysis Is Not Required for Tubulin Oligomer Formation. The tubulin oligomers that are induced by $p150^{glued}$ have a linear, curved formation that could act as a building block for tubulin polymerization. Similar observations have been made for CLIP-170 (19). This curved morphology of tubulin oligomers can also be observed in GDP-tubulin rings (20), which is actually the preferred nucleotide state for depolymerized tubulin (21). Furthermore, curved protofilaments are observed at the depolymerizing ends of microtubules (17, 22, 23). Therefore, we asked whether the hydrolysis of GTP occurs coincidently with tubulin oligomerization. For this purpose, we measured the concentration of inorganic phosphate (P_i) released in the presence

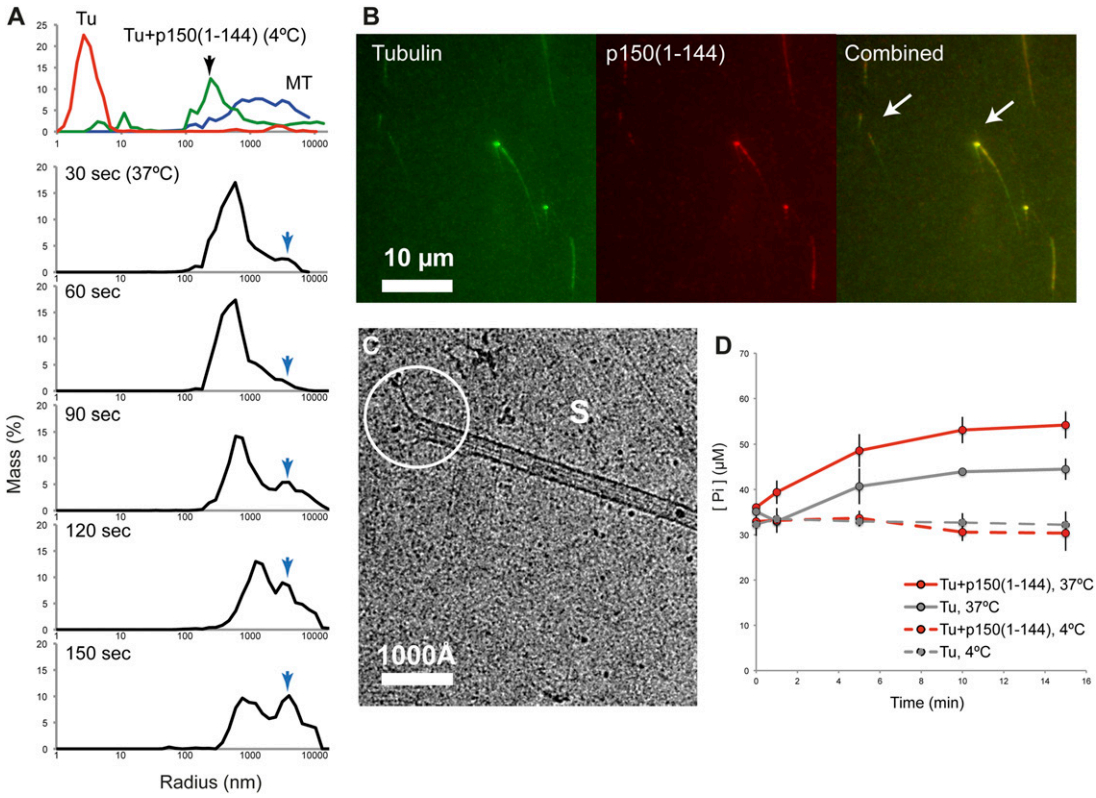

Fig. 4. Intermediates of tubulin polymerization induced by p150(1–144). (*A*) DLS measurements of the mixture of tubulin and p150(1–144). (First row) The control scattering profile of tubulin at 4 °C (red), tubulin with p150(1–144) (green), and microtubule at 37 °C (blue). (second to sixth row) Scattering profiles of the mixture of tubulin-p150(1–144) after incubation at the indicated time points at 37 °C. The blue arrow traces the growth of the microtubules and sheets. (*B*) Copolymerization of p150(1–144) and tubulin into microtubules at 5 min observed by fluorescence microscopy. Two examples of the colocalization of CAP-Gly and tubulin are indicated by arrows. (*C*) Cryo-EM observation of tubulin and p150(1–144) copolymerization 5 min after mixing. S, sheet together with thin fibrils, which are precursors of protofilaments. The active end of a microtubule is indicated with a white circle. (*D*) GTPase activity measurements of tubulin alone (gray, dotted line), tubulin with p150(1–144) (red, dotted line) at 4 °C, and the corresponding curves at 37 °C (solid lines, respectively). Error bars (SD) are calculated from three independent measurements.

of tubulin and p150(1–144) during the formation of curved oligomers. Surprisingly, we did not observe any significant differences in [P_i] at any time of incubation (Fig. 4*D*, dotted lines): 32.7 μM (SD 2.4) (Tu only) vs. 32.1 μM (SD 2.0) [Tu plus p150 (1–144)]. It indicates that GTP hydrolysis is not coupled to tubulin oligomerization. We also observed that tubulin-p150(1–144) oligomerizes in the presence of GMPCPP (a nonhydrolyzable analog of GTP) and that the oligomers retained their curved shape (Fig. S7). Thus, the observed curved tubulin oligomers are not due to GTP hydrolysis. On the contrary, the GTPase activity of tubulin was activated in the presence of p150 (1–144) more than the tubulin control (Fig. 4*D*, red solid line) after the initiation of tubulin polymerization, suggesting that GTP hydrolysis is required only when the incorporation of the tubulin oligomers into the microtubule lattice occurs.

Deletion of Tubulin E-Hook Activates Tubulin Polymerization. Our assays showed that the binding to CAP-Gly is mediated by tubulin E-hooks, in agreement with previous biochemical reports (6–9, 13, 24), and that the coverage of E-hooks by the basic extension activates tubulin polymerization. A similar activation of tubulin polymerization was observed by subtilisin-treated tubulin alone (Fig. S8) (25, 26). The resulting polymerized products showed bundling of the microtubules or open and connected sheets under EM (Fig. S8*B*), supporting the notion that the E-hooks shield tubulins from the lateral connection. Altogether, these findings suggest the importance of E-hooks to control tubulin polymerization kinetics using a negatively charged patch as a shield. The positively charged CAP-Gly fragments may modulate the tubulin polymerization by neutralizing the electrostatic shield of the E-hooks.

Discussion

Our study describes the interaction of tubulin E-hooks with $p150^{glued}$ from a structural point of view and seeks to describe the relationship of the molecular interaction with tubulin polymerization activity. $p150^{glued}$ CAP-Gly plus its adjacent basic patches recognizes the negative electrostatic surface of the tubulin acidic E-hooks. Its binding surface differs from other microtubule-binding proteins in the endosomal recruitment pathway. The basic patches affect tubulin self-assembly through interactions with tubulin's E-hooks. From our observations, we surmise a possible role of tubulin E-hooks in the context of CAP-Gly interaction. Namely, CAP-Gly and its basic patches may work as a cross-linker of tubulins. This crosslinking effect could be seen as oligomeric association when tubulin is not spontaneously associable (4 °C). Upon the change of the temperature to 37 °C, lateral association of protofilaments may be immediately activated. These two directional associations may lead to the acceleration of the polymerization. The effect is likely more efficient when CAP-Gly forms dimers (11), presumably due to the increase of the local concentration. We in fact observed a stronger local clustering of tubulin oligomers in the presence of the dimeric protein (Fig. 3). This bridging could serve as a stabilizer for tubulin to adopt a polymerizable conformation. In a cellular environment, this nucleation mechanism of $p150^{glued}$ may be facilitated when microtubules undergo the phase change from rapid shrinkage to growth. Efficient growth of the microtubules at the plus ends can be achieved if

tubulin oligomers are used as the basic building block. Similar models were suggested for other +TIP proteins (18), and a comprehensive analysis combining these components is necessary.

Implications of the Nonoverlapping Recognition of p150^{glued}, EB, and Dynein and of the Surfing Activity of p150^{glued}. Our structural analysis directly identified the interaction interface between p150^{glued} CAP-Gly and tubulin E-hooks. Interestingly, this binding surface on tubulin is distinct from those of EBs and dynein (Fig. 2). CAP-Gly recognizes tubulin E-hooks protruding from the outer surface of the microtubule whereas EBs recognize the nucleotide-binding pocket at the groove between the microtubule protofilaments. Dynein binds to an area closer to helices H11/H12 of tubulin, which is also the binding site for the other major microtubule-motor protein kinesin (27) (Fig. 2). Moreover, p150^{glued} has been reported to form a complex with EB1 and CLIP-170, and this +TIPs complex would track the plus ends of microtubules (1). Our finding that the binding sites of these three microtubule-associated proteins do not sterically hinder each other may facilitate a smooth bridging of the plus-end tracking and subsequent vesicle tethering to the dynein motor.

p150^{glued} has been reported to diffuse one-dimensionally along the microtubule surface, termed surfing/skating (12, 28). Considering the main function of p150^{glued} as an anchor for vesicles at the plus end of microtubules (29–32), it is conceivable that the surfing activity is a way of maximizing the chance of encountering EB proteins that directly recognize GTP-tubulin at the end of microtubules. Our study provides a molecular basis for this surfing mechanism. E-hooks, which are incorporated into the microtubule surface, provide a periodic array of negative electrostatic charges. CAP-Gly, with its basic patches, recognizes this surface. CAP-Gly also has a specific interaction with E-hooks, which can ensure efficient binding to microtubules. E-hooks give an opportunity for CAP-Gly to diffuse laterally to the next binding site by providing the continuous charged surface.

The Role of Tyrosinated Tubulin for p150^{glued}. It has been reported that p150^{glued} CAP-Gly domains bind preferably to alpha tubulin that is tyrosinated at the C-terminal E-hook (7). Tubulin tyrosination occurs in its depolymerized form (33) and so freshly incorporated alpha tubulin harbors the modification at microtubule plus ends. This biased distribution of tyrosinated tubulin is likely the key for the microtubule plus-end recognition by CAP-Gly (7, 34). In our assays, p150^{glued} CAP-Gly core has a higher affinity to the tyrosinated alpha E-hook compared with the detyrosinated E-hook and beta E-hook (Table 1), but the basic extensions increase the binding affinity of CAP-Gly fragments to other E-hooks. CAP-Gly prefers tyrosinated tubulin to bias itself toward the plus ends of microtubules. The situation in a cell, however, might be more complex. E-hooks are variable in isoforms in addition to the diverse decoration by posttranslational modifications. The weak interaction through basic extensions might play a role for reinforcing the affinity of p150^{glued} to microtubules. Further studies are needed to understand the functions of different tubulin isoforms in the context of posttranslational modifications.

Materials and Methods

Recombinant proteins of p150^{glued} fragments, CLIP-170, EB1, and KH are expressed in *E. coli*. Protein purifications and subsequent biochemical analyses were carried out as described in *SI Material and Methods*. Details of electron microscopic analyses are also found in *SI Material and Methods*, as well as in Fig. S9.

ACKNOWLEDGMENTS. We thank Dr. Elena Conti and Dr. Wolfgang Baumeister for resources and support and the Core Facility of the Max Planck Institute of Biochemistry for MGC clones and peptide synthesis; Dr. Jürg Müller for a generously sharing Histone H2A protein; and Dr. Tanvir Shaikh, Dr. Yoko Y. Toyoshima, Dr. Christian Biertümpfel, Dr. Petra Schwille, and Dr. Sven Vogel for insightful discussion and careful readings of the manuscript. We also thank Dr. Giovanni Cardone for valuable discussions about image processing and Dr. Charles Sindelar for sharing his script for the conversion of parameters between different software. This study was supported by the Max Planck Society for the Advancement of Science and the Deutsche Forschungsgemeinshaft DFG through a grant within the SPP1464, GRK1721, and MI 1745/1.

1. Akhmanova A, Steinmetz MO (2008) Tracking the ends: A dynamic protein network controls the fate of microtubule tips. *Nat Rev Mol Cell Biol* 9(4):309–322.
2. Cronin MA, Schwarz TL (2012) The CAP-Gly of p150: One domain, two diseases, and a function at the end. *Neuron* 74(2):211–213.
3. Watson P, Stephens DJ (2006) Microtubule plus-end loading of p150(Glued) is mediated by EB1 and CLIP-170 but is not required for intracellular membrane traffic in mammalian cells. *J Cell Sci* 119(Pt 13):2758–2767.
4. Lansbergen G, et al. (2004) Conformational changes in CLIP-170 regulate its binding to microtubules and dynactin localization. *J Cell Biol* 166(7):1003–1014.
5. Ligon LA, Shelly SS, Tokito M, Holzbaur ELF (2003) The microtubule plus-end proteins EB1 and dynactin have differential effects on microtubule polymerization. *Mol Biol Cell* 14(4):1405–1417.
6. Hayashi I, Wilde A, Mal TK, Ikura M (2005) Structural basis for the activation of microtubule assembly by the EB1 and p150Glued complex. *Mol Cell* 19(4):449–460.
7. Peris L, et al. (2006) Tubulin tyrosination is a major factor affecting the recruitment of CAP-Gly proteins at microtubule plus ends. *J Cell Biol* 174(6):839–849.
8. Honnappa S, et al. (2006) Key interaction modes of dynamic +TIP networks. *Mol Cell* 23(5):663–671.
9. Weisbrich A, et al. (2007) Structure-function relationship of CAP-Gly domains. *Nat Struct Mol Biol* 14(10):959–967.
10. Bieling P, et al. (2008) CLIP-170 tracks growing microtubule ends by dynamically recognizing composite EB1/tubulin-binding sites. *J Cell Biol* 183(7):1223–1233.
11. Lazarus JE, Moughamian AJ, Tokito MK, Holzbaur ELF (2013) Dynactin subunit p150 (Glued) is a neuron-specific anti-catastrophe factor. *PLoS Biol* 11(7):e1001611.
12. Culver-Hanlon TL, Lex SA, Stephens AD, Quintyne NJ, King SJ (2006) A microtubule-binding domain in dynactin increases dynein processivity by skating along microtubules. *Nat Cell Biol* 8(3):264–270.
13. Kobayashi T, Shiroguchi K, Edamatsu M, Toyoshima YY (2006) Microtubule-binding properties of dynactin p150 expedient for dynein motility. *Biochem Biophys Res Commun* 340(1):23–28.
14. Sui H, Downing KH (2010) Structural basis of interprotofilament interaction and lateral deformation of microtubules. *Structure* 18:1022–1031.
15. Redwine WB, et al. (2012) Structural basis for microtubule binding and release by dynein. *Science* 337(6101):1532–1536.
16. Maurer SP, Fourniol FJ, Bohner G, Moores CA, Surrey T (2012) EBs recognize a nucleotide-dependent structural cap at growing microtubule ends. *Cell* 149(2):371–382.
17. Mandelkow EM, Mandelkow E, Milligan RA (1991) Microtubule dynamics and microtubule caps: A time-resolved cryo-electron microscopy study. *J Cell Biol* 114(5):977–991.
18. Slep KC, Vale RD (2007) Structural basis of microtubule plus end tracking by XMAP215, CLIP-170, and EB1. *Mol Cell* 27(6):976–991.
19. Arnal I, Heichette C, Diamantopoulos GS, Chrétien D (2004) CLIP-170/tubulin-curved oligomers coassemble at microtubule ends and promote rescues. *Curr Biol* 14(23):2086–2095.
20. Nicholson WV, Lee M, Downing KH, Nogales E (1999) Cryo-electron microscopy of GDP-tubulin rings. *Cell Biochem Biophys* 31(2):175–183.
21. Tran PT, Joshi P, Salmon ED (1997) How tubulin subunits are lost from the shortening ends of microtubules. *J Struct Biol* 118(2):107–118.
22. Moores CA, et al. (2002) A mechanism for microtubule depolymerization by KinI kinesins. *Mol Cell* 9(4):903–909.
23. Asenjo AB, et al. (2013) Structural model for tubulin recognition and deformation by kinesin-13 microtubule depolymerases. *Cell Reports* 3(3):759–768.
24. Bu W, Su L-K (2003) Characterization of functional domains of human EB1 family proteins. *J Biol Chem* 278(50):49721–49731.
25. Sackett DL, Bhattacharyya B, Wolff J (1985) Tubulin subunit carboxyl termini determine polymerization efficiency. *J Biol Chem* 260(1):43–45.
26. Peyrot V, Briand C, Andreu JM (1990) C-terminal cleavage of tubulin by subtilisin enhances ring formation. *Arch Biochem Biophys* 279(2):328–337.
27. Mizuno N, et al. (2004) Dynein and kinesin share an overlapping microtubule-binding site. *EMBO J* 23(13):2459–2467.
28. King SJ, Schroer TA (2000) Dynactin increases the processivity of the cytoplasmic dynein motor. *Nat Cell Biol* 2(1):20–24.
29. Kim H, et al. (2007) Microtubule binding by dynactin is required for microtubule organization but not cargo transport. *J Cell Biol* 176(5):641–651.
30. Chevalier-Larsen ES, Wallace KE, Pennise CR, Holzbaur ELF (2008) Lysosomal proliferation and distal degeneration in motor neurons expressing the G59S mutation in the p150Glued subunit of dynactin. *Hum Mol Genet* 17(13):1946–1955.
31. Moughamian AJ, Holzbaur ELF (2012) Dynactin is required for transport initiation from the distal axon. *Neuron* 74(2):331–343.
32. Kardon JR, Reck-Peterson SL, Vale RD (2009) Regulation of the processivity and intracellular localization of Saccharomyces cerevisiae dynein by dynactin. *Proc Natl Acad Sci USA* 106(14):5669–5674.
33. Janke C, Bulinski JC (2011) Post-translational regulation of the microtubule cytoskeleton: Mechanisms and functions. *Nat Rev Mol Cell Biol* 12(12):773–786.
34. Mishima M, et al. (2007) Structural basis for tubulin recognition by cytoplasmic linker protein 170 and its autoinhibition. *Proc Natl Acad Sci USA* 104(25):10346–10351.

Supporting Information

Wang et al. 10.1073/pnas.1403135111

SI Discussion

To understand the binding of cytoskeleton-associated protein glycine-rich (CAP-Gly) and tubulins in our experimental system, we chemically cross-linked p150^{glued} CAP-Gly fragments to microtubules that were treated with subtilisin. Subtilisin digests the E-hooks of beta and alpha tubulin in a time-dependent manner (Fig. S2*A*). After 30 min of digestion, in which subtilisin removes only the E-hook of beta tubulin, we observed a decrease of cross-linked products. After 4–6 h of incubation, when also alpha tubulin E-hooks are digested, the cross-linking of CAP-Gly to tubulin is no longer detectable, indicating that the p150^{glued} CAP-Gly-microtubule interaction was maintained by tubulin E-hooks. The binding affinities of the peptides (alpha, tyrosinated, and detyrosinated tubulin E-hooks and beta tubulin E-hooks) and p150^{glued} fragments were further determined by a binding assay using fluorescence correlation spectroscopy (Table 1). This binding was also confirmed by cross-linking CAP-Gly to chemically synthesized E-hook peptides (Fig. S2*D*). Next, we determined the stoichiometry of CAP-Gly-tubulin complexes using a microtubule-pelleting assay with p150^{glued} CAP-Gly and polymerized, taxol-stabilized microtubules. The binding of CAP-Gly itself to microtubules appears to be fairly weak (Fig. S1*A*, marked with an *), but CAP-Gly containing the upstream/downstream basic patches increased the binding affinity. The quantitative pelleting assay of p150(1–144) and microtubules shows a K_d of 2.2 μM, with a stoichiometry of two proteins per tubulin dimer (Fig. S2*A*). Altogether, our experiments indicate that p150^{glued} CAP-Gly recognizes both alpha and beta tubulins at saturation levels. The stoichiometry of 2 was also used to define the asymmetric unit for the 3D reconstruction.

SI Materials and Methods

Protein Preparation and Purification. For all cloned constructs, DNA was obtained from the Mammalian Gene Collection (MGC, Source BioScience LifeSciences) or the Berkeley Drosophila Genome Project (BDGP) Gold cDNA Collection (*Drosophila* Genomic Resource Center) and further modified by PCR. Human p150^{glued} (25–105, 1–105, 25–144, 1–144), CLIP-170 (CLIP-170L, 1–350; CLIP-170S, 57–210), and end-binding protein 1 (EB1) (1-133) were expressed as His-tagged recombinant proteins using the *Escherichia coli* BL21 (DE3) Gold strain. For p150(106–144) and *Drosophila* kinesin head (KH, 1–342), the fragment was expressed as a SUMO fusion protein, and SUMO tag was cleaved using Senp2 protease. Proteins were purified using Ni^{2+}-affinity chromatography (HisTrap; GE Healthcare) followed by MonoS ionic exchange chromatography (GE Healthcare) and gel-filtration chromatography (Superdex 75; GE Healthcare).

Tubulin was purified from porcine brains or purchased from Cytoskeleton, Inc. Histone H2A is a generous gift from Jürg Müller (Max Planck Institute of Biochemistry, Martinsried, Germany). Proteins were stored in 20 mM Pipes-NaOH (pH 6.8), 1 mM $MgCl_2$, 1 mM EGTA, 100 mM NaCl, and 1 mM DTT or BRB80 [80 mM Pipes-Na (pH 6.8), 1 mM $MgCl_2$, 1 mM EGTA] supplemented with 1 mM DTT. All experiments were performed in BRB80 buffer or with BRB80 supplemented with an additional 35 mM or 70 mM KCl. Ionic strengths of the buffers were measured using the conductivity detector of an Aekta Purifier system (GE Healthcare) calibrated with NaCl solutions of known concentrations. BRB80 was corresponded to ∼80 mM, BRB80 plus 35 mM KCl to 115 mM, and BRB80 plus 70 mM KCl to 150 mM.

Kinetics Measurement of Tubulin Polymerization. For measurement of microtubule polymerization, a Bio Photometer plus (Eppendorf) spectrophotometer was used. The copolymerization assays below the critical concentration of tubulin were performed with 2 μM tubulin with 1 μM of the protein fragments, 1 mM GTP, and 8% (vol/vol) DMSO in BRB80, with ionic strengths corresponding to 80/115/150 mM. The assays were performed in a room with controlled temperature at 37 °C. There was a systematic error of the perturbation of scattering for the first 3 min, presumably because of the experimental setup; therefore, the initial time was not considered for the measurement. The measurement was performed up to 30 min and repeated three times. For the measurement of the tubulin polymerization above the critical concentration, 10 μM tubulin, 5 μM protein fragments, 1 mM GTP, and 8% DMSO were mixed in BRB80, and the measurements were carried out as described above.

Dynamic Light Scattering. The measurement was performed using a Wyatt NanoStar (Wyatt Technology). For each measurement, a 10-μl sample was prepared containing 1 mM GTP and 10 μM tubulin as a control, and 5 μM p150(1–144) was added for the test experiments. The measurements were repeated every 3 s, and the results were averaged over 10 measurements. To follow the transition of different species during tubulin polymerization, data corresponding to a time of 30 s were averaged. The temperature was set to either 4 °C or 37 °C as indicated. Concentrations of samples were adjusted to avoid detector saturation.

Fluorescence Microscopy. For labeling, p150^{glued} CAP-Gly was modified (C81S), and an additional cysteine was inserted at residue 105 because labeling of the wild-type constructs caused a loss of the tubulin nucleator activity: i.e., no oligomeric formation was observed. Modified protein was purified as described above. Labeling was performed using atto565-maleimide, and the activity of the labeled protein was confirmed by kinetics experiments as well as the observation of the curved tubulin oligomers. Labeled tubulin was purchased from Cytoskeleton, Inc. An upright epifluorescence microscope (Zeiss) was used for image acquisition equipped with a filter set (FITC and TRITC) and an EM CCD camera (X-ion Andor). MetaMorph was used for microscope control and image acquisition.

Phosphate Release Detection. The release of phosphate was measured by using PhosFree Phosphate Assay BIOCHEM kit (BK050) from Cytoskeleton Inc. Then, 20 μM tubulin was mixed with 20 μM p150(1–144) in a total volume of 50 μl. The reaction was quenched at 0 min, 1 min, 5 min, 10 min, and 15 min after the samples were mixed at 4 °C and 37 °C. The quenched mixture was centrifuged at 20,000 × *g*, and the supernatant was used for detection of phosphate using malachite green staining and absorbance measurements at λ = 650 nm according to the manufacturer's manual. To minimize errors, we used the same batches of GTP and tubulin for all measurements. The measurements were repeated three times.

Microtubule-Binding Assay. Polymerized and taxol-stabilized microtubules (2 μM) were mixed with various concentrations of p150^{glued} proteins. After incubating for 20 min at room temperature, the 40-μL mixture was ultracentrifuged for 20 min at 280,000 × *g* at 25 °C. The supernatant was recovered, and the pellet was carefully washed with BRB80 once. p150^{glued}-CAP-Gly bound to microtubules was quantified using SDS/PAGE and ImageJ. For assessment of the simultaneous microtubule

bindings of p150(1–144), EB1, and KH, microtubules were polymerized using GTPgammaS instead of GTP for ensuring EB1 binding. Then, microtubules (2 μM) were mixed with the proteins (20 μM), and the pelleting assay was performed as described above.

EDC Cross-Linking. For the cross-linking assay, 5 μM polymerized/unpolymerized tubulins were mixed with proteins, and 1-Ethyl-3-[3-dimethylaminopropyl]carbodiimide hydrochloride (EDC) (Fisher) was added to a final concentration of 5 mM. Samples were incubated either on ice or at room temperature for 1 h. The EDC reaction was stopped by adding SDS sample buffer.

Subtilisin Treatment on Microtubule and Tubulin. For the treatment of microtubules, 15 μM taxol-stabilized microtubules were mixed with 5.6 μM subtilisin (Sigma Aldrich) and incubated for 1 min, 10 min, 30 min, 60 min, 120 min, 240 min, 360 min, or 480 min at room temperature or 10 min, 30 min, 60 min, or 90 min at 37 °C. It is known that the beta E-hooks are cleaved first, followed by the alpha E-hooks (1). The cleavage of E-hooks was confirmed by band shifts in SDS/PAGE (4–20% gradient) and Western blotting against anti-alpha tubulin, clone YL1/2 (Merck Millipore) that recognizes alpha tubulin E-hooks (Fig. S2*C*). The enzymatic reaction was stopped by adding 2.5 mM PMSF. Subtilisin-treated microtubules were further purified by ultracentrifugation, and the pellet was resuspended gently to achieve the desired concentration for further experiments. For the treatment of tubulins, 20 μM tubulin was mixed with 7.4 μM subtilisin, and the mixture was incubated for 30 min in 30 °C followed by an addition of 2.5 mM PMSF.

Peptide Binding Assay. Peptides were synthesized by the Max Planck Institute of Biochemistry Core Facility. We prepared peptides corresponding to the tyrosinated E-hook of alpha tubulin (alpha CY, biotin-GSSVEGEGEEEGEEY), the detyrosinated (glutamated) tail of alpha tubulin (alpha CE, biotin-GSSVEGEGEEEGEE), and the E-hook of beta tubulin (beta C, biotin-GSGEFEEEGEEDEA). Then, peptides (25 μM) and $p150^{glued}$ proteins (100 μM) were mixed, and chemical cross-linking assays were performed using EDC. The results were evaluated on SDS/PAGE.

Fluorescence Correlation Spectroscopy. Fluorescence correlation spectroscopy was carried out using a system previously described (2). Peptides labeled with atto488 at the N termini were synthesized by the Max Planck Institute of Biochemistry Core Facility. Peptides (1 nM) and $p150^{glued}$ fragments (0.01–100 μM) were mixed in BRB80 and allowed to reach steady-state binding for 20 min before the measurement. Data were acquired for 10 min using a laser power of 15 μW. All analysis was carried out using custom-written programs in MATLAB. To calculate diffusion coefficients of the protein–peptide complexes, the focus size was fixed using a 400 $\mu m^2/s$ diffusion coefficient of atto488 free carboxylic acid (taken from http://www.picoquant.com/appnotes.htm).

Sample Preparations for Electron Microscopy. For the observation of tubulin oligomerization, tubulin (10 μM) was mixed with proteins (10 μM) and incubated for 5 min on ice. The sample was applied to the grid without dilution because dilution causes the dissociation of oligomers. For the observation of polymerization intermediates, tubulin (10 μM) and proteins (10 μM) were mixed and incubated at 37 °C for 5 min. The samples were immediately vitrified using a Vitrobot (FEI). For the observation of the microtubule–protein mixture, taxol-stabilized microtubule (2 μM) was mixed with proteins (20 μM), and the sample was vitrified immediately.

Electron Microscopy Operation. For negative-stain EM, carbon-coated and freshly glow-discharged grids were prepared. Then, 5 μL of sample were applied to the grids. Excess solution was removed by filter paper followed by rinsing with H_2O, and staining with two drops of 1% uranyl acetate. Samples were observed with a CM200-FEG (FEI) operating at 160 kV with the nominal magnification of 38,000×, corresponding to 2.78 Å per pixel.

For cryo-EM, holey carbon grids purchased from Quantifoil were used. After glow discharge, the samples were applied to the grids, and vitrification was immediately carried out using a vitrobot (FEI). For observation, a Tecnai F20 (FEI) was used with an acceleration voltage of 200 kV and with a nominal magnification of 50,000× corresponding to a pixel size of 2.21 Å per pixel. The images were taken with a CCD camera (FEI, Eagle) with a defocus range of 1–3 μm.

Image Processing. Image processing was carried out using BSOFT (3), SPIDER (4), and IHRSR (5) for single-particle microtubule reconstruction.

For cryo-EM image processing, defocus values of the collected images were measured using ctffind3 (6), and the contrast transfer function (CTF) was corrected by phase-flipping. Microtubules were computationally boxed out to squares with a size of 200 × 200 pixels (corresponding to 442 × 442 Å) by tracing the central axis of the tubes. Opened or bundled microtubules were not selected. The selected microtubules were tested by applying multireference alignment using the reprojections of available microtubule maps (EMDB ID: emd_5193/5194/5195/5196) with various protofilament numbers, namely microtubules with 13 protofilaments, 14 protofilaments, 15 protofilaments, and 16 protofilaments as references, and the numbers of the protofilaments of individual boxes were determined using the highest cross-correlation value of the alignments. The consistency of the protofilament number within a filament and the characteristic Moiré patterns based on the protofilament numbers were taken into consideration as well.

$p150^{glued}$ binds to every tubulin monomer, confirmed by chemical cross-linking and pelleting assays as well. This observation facilitated the use of the most commonly found 14-protofilament microtubules as test samples, and further reconstructions were performed using 14-protofilament microtubules.

Reconstructions were done using the iterative helical real space reconstruction (IHRSR) approach by applying the helical parameters of microtubules. The helical parameters were defined to be 231° azimuthal rotation and 2.98 Å rise per asymmetric unit as a tubulin monomer. We used 56,000 asymmetric particles, for the final reconstruction of p150(1–105), 52,700 asymmetric particles for p150(25–144), and 12,000 asymmetric particles for p150(25–105) reconstructions. A cylindrical density of the same size as the 14-protofilament microtubule was created as an initial volume, and the iterative reconstruction was performed 50 times. During each iteration, a reference was created by calculating reprojections of the reconstruction from the previous cycle by rotating every 4° toward the azimuthal direction, which produced 90 reference images. The new reconstruction was created by back projection, and then the helical parameters were imposed. As a refinement, the number of the reference images was increased to 3,690 images including out-of-plane tilt alignment, and the refinement process was iterated for a further 20 times. The amplitudes of high frequency components in the CAP-Gly1-105-microtubule reconstruction were adjusted by fitting helically symmetrized atomic models of tubulin (PDB ID code 1TUB) into the EM envelope as reference. By adjusting the amplitudes, the density of the CAP-Gly1-105 weakened; therefore, the maps used for the detection of the protein decoration were not amplitude-corrected. The resolution of the map was measured by calculating the Fourier shell correlation (FSC) of two reconstructions that were individually calculated from the initial cylindrical volumes. Before the FSC calculations, a mask was

created by using the volumes of the reconstructions, generously including surrounding noise densities, followed by five times of a dilation and smoothing procedure provided by bsoft, and the mask was applied to the reconstruction to be compared. The resolution was estimated to be 9.7 Å according to FSC (0.5) criteria (Fig. S9*B*) for the p150(1–105)–microtubule complex and 10.2 Å for the p150(25–144)–microtubule complex.

Atomic models of tubulin (PDB ID code 1TUB) were used for molecular fitting into the microtubule-CAP-Gly1-105 reconstruction. For the mapping of the dynein and Mal3 (EB1) binding regions on the microtubule, the EM maps of dynein-microtubule (EMDB ID 5439) and Mal3-microtubule (EMDB ID 2005) were used. In both cases, we manually fit the maps using UCSF Chimera (University of California, San Francisco).

1. Redeker V, Melki R, Promé D, Le Caer JP, Rossier J (1992) Structure of tubulin C-terminal domain obtained by subtilisin treatment: The major alpha and beta tubulin isotypes from pig brain are glutamylated. *FEBS Lett* 313(2):185–192.
2. Müller BK, Zaychikov E, Bräuchle C, Lamb DC (2005) Pulsed interleaved excitation. *Biophys J* 89(5):3508–3522.
3. Heymann JB, Belnap DM (2007) Bsoft: image processing and molecular modeling for electron microscopy. *J Struct Biol* 157(1):3–18.
4. Frank J, et al. (1996) SPIDER and WEB: Processing and visualization of images in 3D electron microscopy and related fields. *J Struct Biol* 116(1):190–199.
5. Egelman EH (2007) The iterative helical real space reconstruction method: Surmounting the problems posed by real polymers. *J Struct Biol* 157(1):83–94.
6. Mindell JA, Grigorieff N (2003) Accurate determination of local defocus and specimen tilt in electron microscopy. *J Struct Biol* 142(3):334–347.

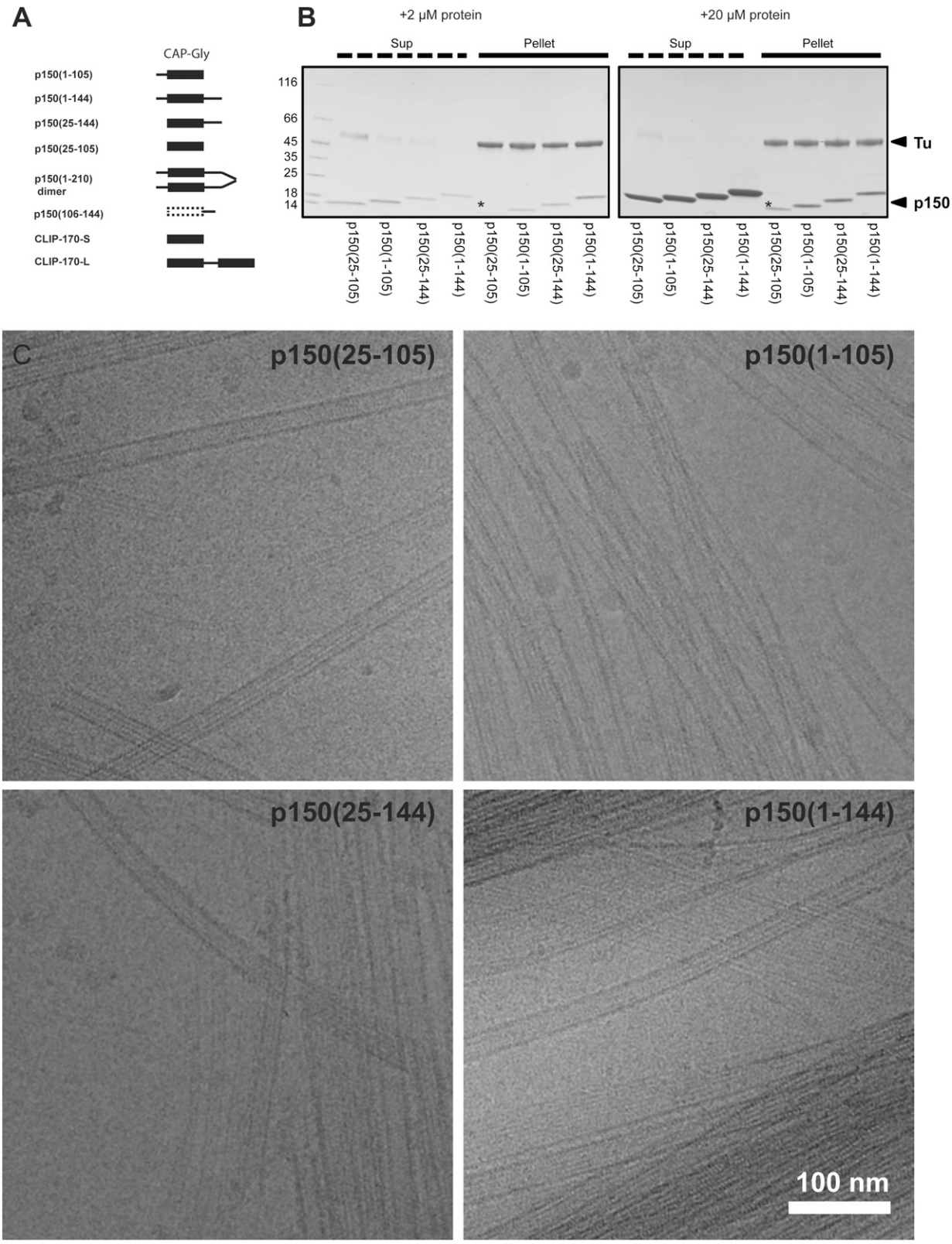

Fig. S1. (*A*) Scheme of the protein fragments used for this study. (*B*) Microtubule pelleting assay showing the affinity of CAP-Gly fragments to microtubules: p150(1–144) > p150(25–144) > p150(1–105) > p150(25–105). Microtubules (2 μM) and individual proteins (2 μM or 20 μM) were used. In the presence of 20-μM protein fragments, the bound proteins to 2 μM microtubules (dimer as a unit) are calculated to be 2.7 μM [p150(25–105), 5.2 μM (p150(1–105), 5.3 μM (p150(25–144)] and 5.2 μM [p150(1–144)]. (*C*) Cryo-EM observations of taxol-stabilized microtubules mixed with $p150^{glued}$-CAP-Gly fragments. CAP-Gly with additional basic patches cause lateral association of microtubules.

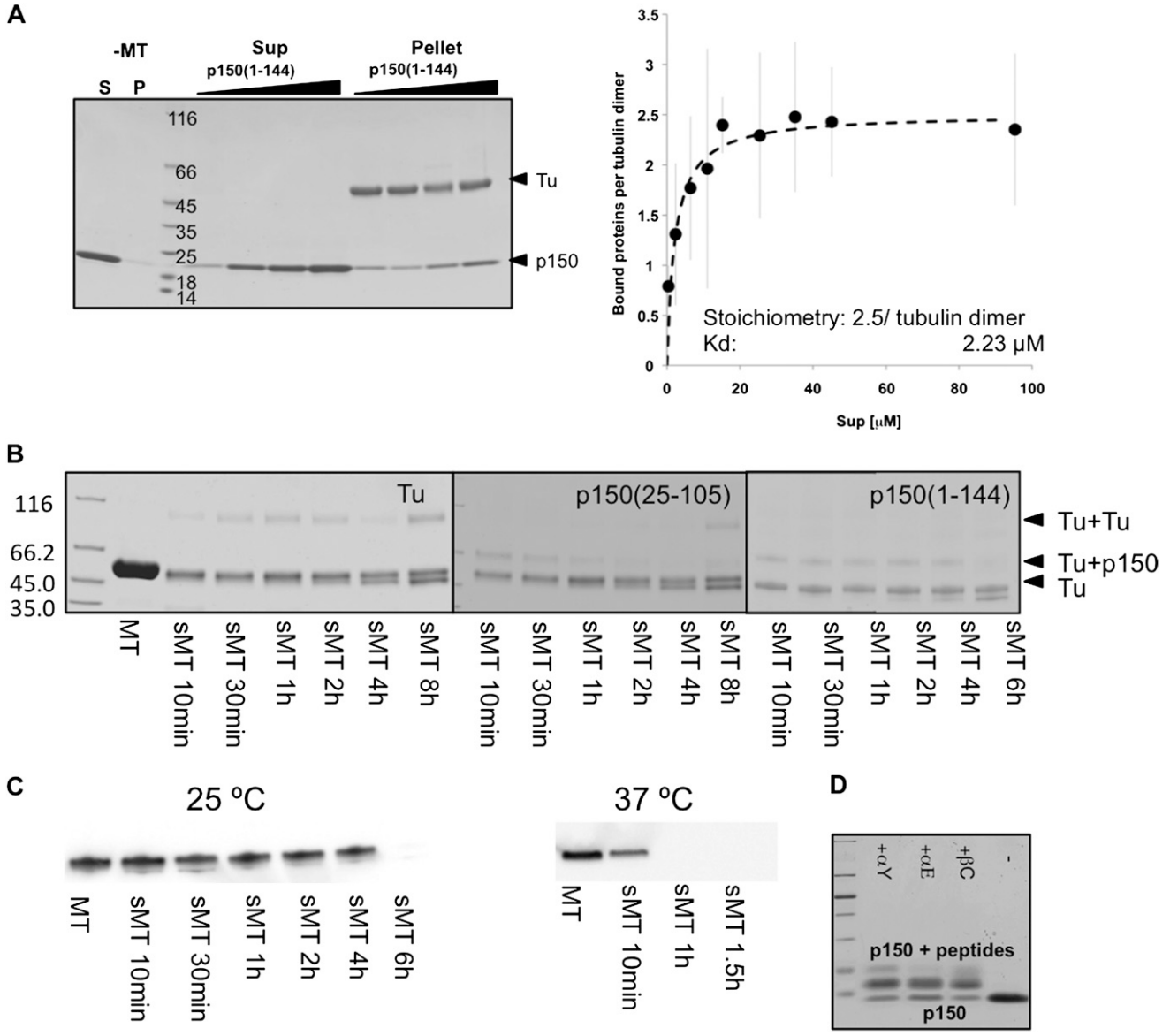

Fig. S2. (*A*, *Left*) An example of the quantitative copelleting assay of microtubules (2 μM) and various concentrations of p150(1–144) (from left: 1 μM, 5 μM, 10 μM, 15 μM). (*Right*) Quantification of the copelleting assay showing the saturation of bound protein at 2.5 mol/tubulin dimer, indicating that p150(1–144) recognizes both alpha and beta tubulin. $K_d = 2.23$ μM. Note that this K_d is a combination of the CAP-Gly binding to alpha and beta tubulin E-hooks. (*B*) EDC cross-linking of subtilisin-treated microtubules and p150glued-CAP-Gly. Cross-linked products are marked with arrowheads. E-hook of beta tubulin is removed in ∼30 min, and the alpha tubulin E-hook is truncated at ∼4–6 h. Concomitantly, the binding of tubulin to $p150^{glued}$-CAP-Gly is lost. (*C*) Western blotting of subtilisin-treated microtubules in 25 °C (*Left*) and 37 °C (*Right*), showing the completion of the cleavage of E-hooks at 6 h (25 °C) and 1 h (37 °C), respectively. For staining, anti-alpha tyrosinated tubulin was used, which detects tyrosine at the end of alpha tubulin E-hooks. (*D*) $p150^{glued}$-CAP-Gly is cross-linked with peptides of alpha [both tyrosinated (marked as αY) and detyrosinated (αE)] and beta E-hooks (βC).

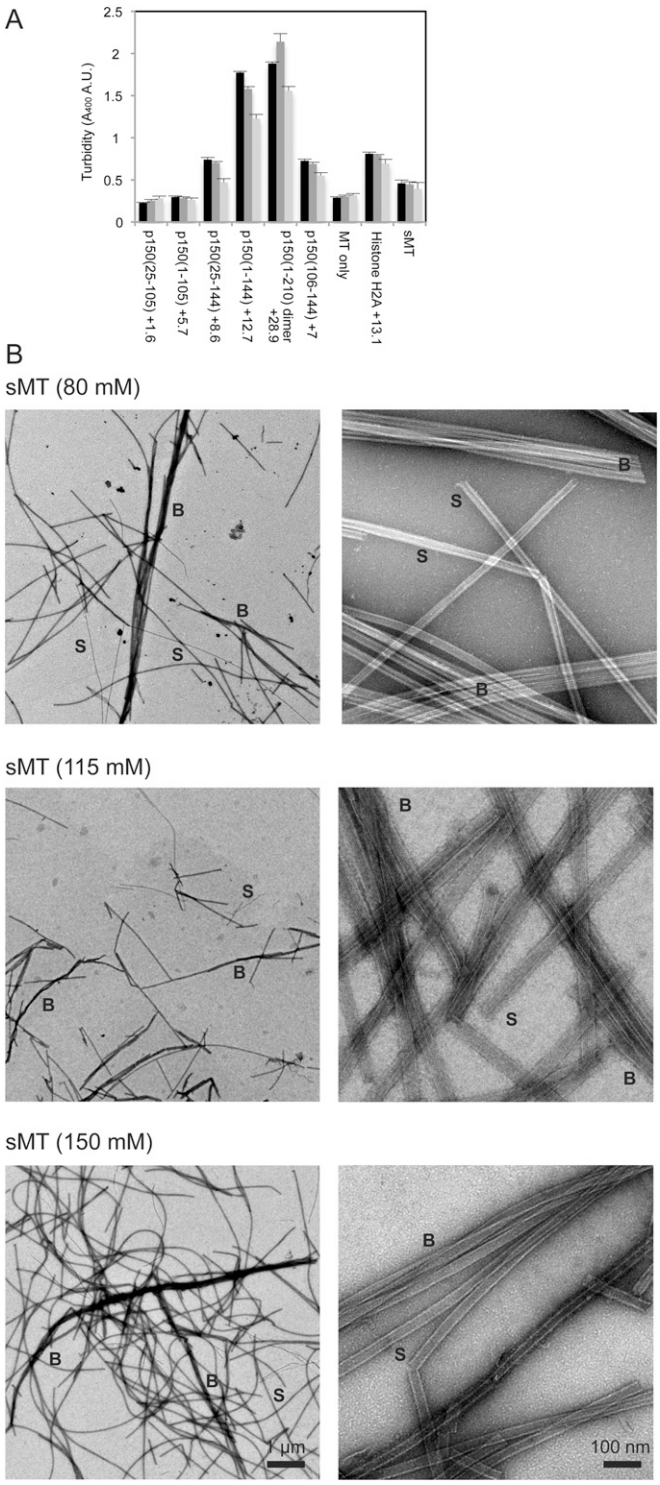

Fig. S3. (*A*) Turbidity change of 10-μM taxol-stabilized microtubules was measured upon additions of the 10-μM protein fragments. The ionic strength of reacting buffer was 80 mM (black bar), 115 mM (dark gray bar), and 150 mM (light gray bar). (*B*) Negative stain EM observations of subtilisin-treated microtubules (2.5 h in 37 °C) showing lateral associations. Examples of bundles and single microtubules are labeled by B and S, respectively.

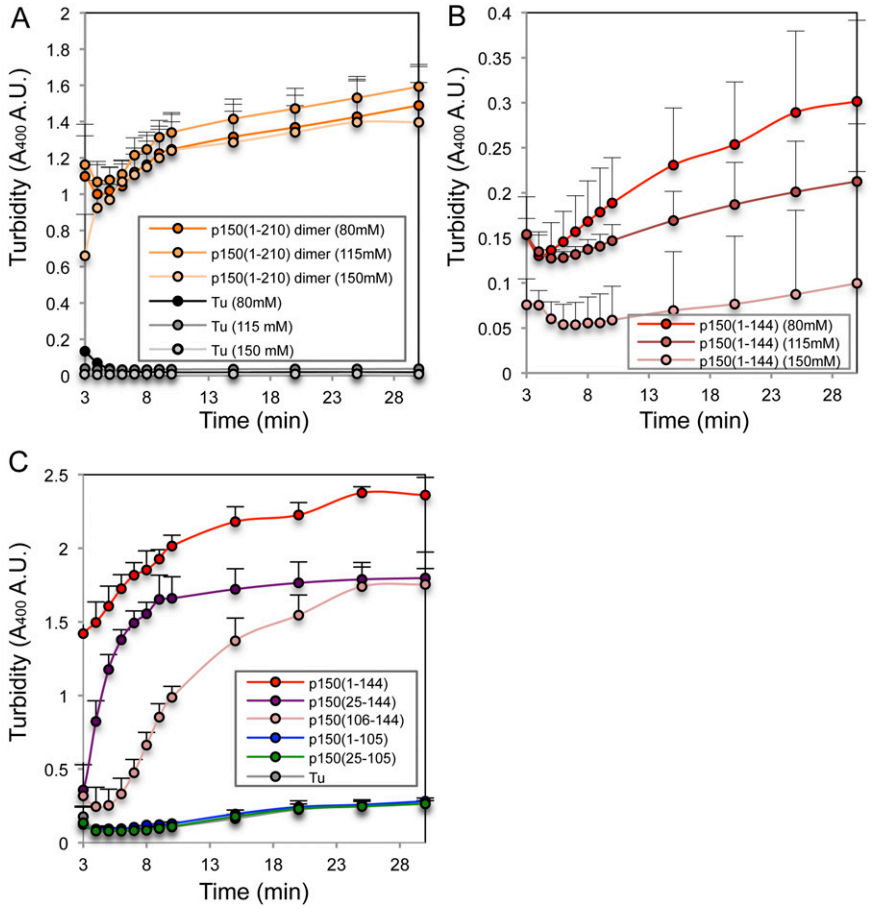

Fig. S4. Turbidity change as a function of time. The turbidity caused by the polymerization of microtubules was measured at an absorbance at 400 nm. The experiments were repeated more than three times for each condition. Only the upper half of error bars are shown for representation purposes. (*A* and *B*) The 2-μM tubulin does not polymerize on its own (gray lines), but, in the presence of 1 μM p150(1–210) dimer, polymerization is promoted as well as in the presence of p150(1–144) to a lesser extent. These phenomena are ionic strength- dependent, which is indicated in the graph legend. (*C*) Tubulin polymerization profiles of 10-μM tubulin and 5-μM p150 fragments. The effect is greater with higher concentrations. Addition of p150(1–105) or p150(25–105) does not increase the turbidity of the microtubule growth, but, with the C-terminal appended basic patches, an increase of the signal occurs.

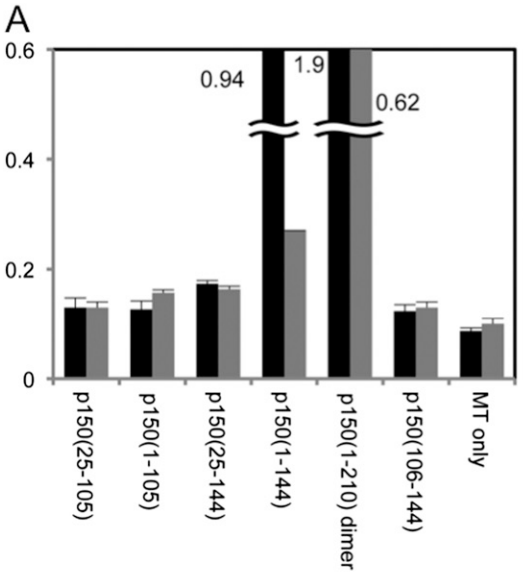

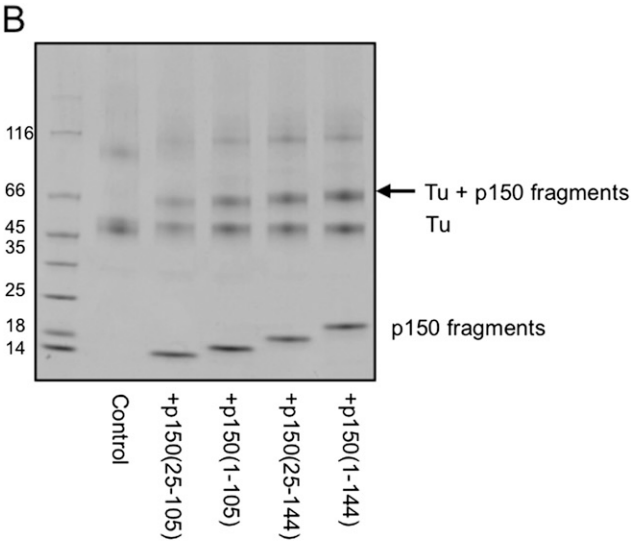

C

Proteins	Net Charge	Oligomer Density
p150(25-105)	+1.6	0
p150 (1-105)	+5.7	0.8 (n=130)
p150(25-144)	+8.6	5.7 (n=130)
p150(1-144)	+12.7	> 17 (n=130)
p150(1-210) Dimer	+28.9	N/A
p150(106-144)	+7	0
C (CLIP-170S)	-	0.8 (n=130)
C (CLIP-170L)	-	3.8 (n=130)
C (Tubulin)	-	0

Fig. S5. (*A*) Turbidity change when 10-μM tubulin and 10-μM protein fragments were mixed together. Black bar, 80-mM ionic strength; gray bar, 115-mM ionic strength. The turbidity change also shows ionic strength dependency, consistent with copolymerization. (*B*) EDC chemical cross-link shows the CAP-Gly fragments cross-linked to unpolymerized tubulin (arrow) at 4 °C. The cross-link reactions happen for both unpolymerized tubulins and polymerized microtubules. (*C*) Density of tubulin oligomers shown in Fig. 3. More than 10 images (1.1×1.1 μm^2) of the tubulin oligomers induced by the proteins were collected and counted per 100×100 nm^2.

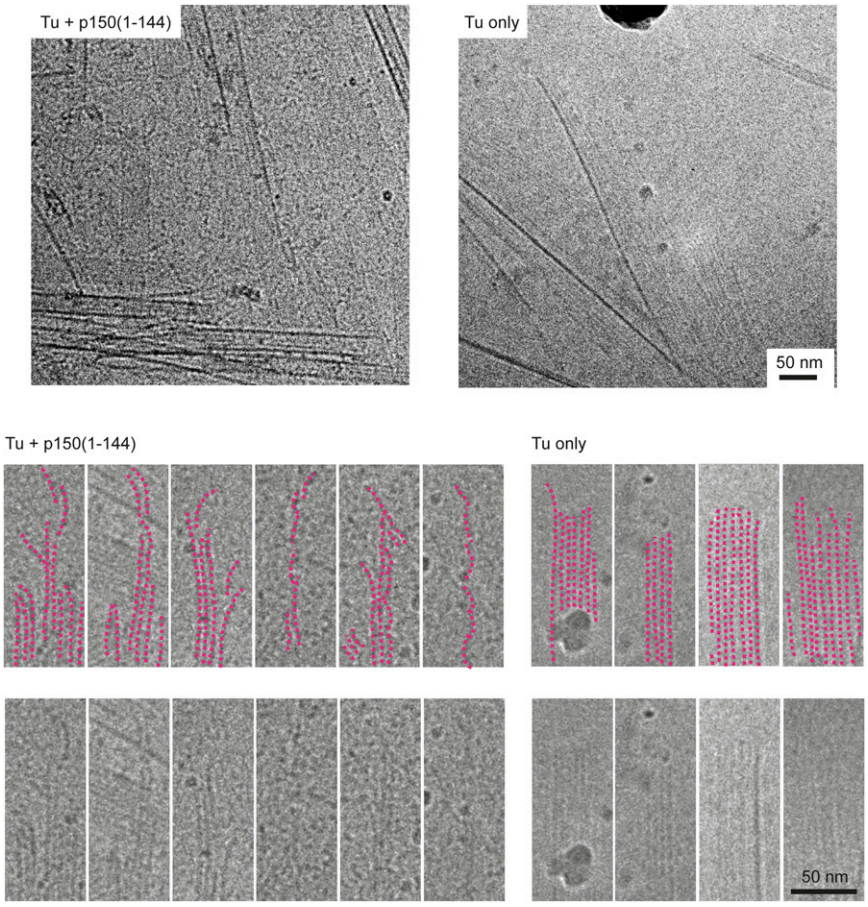

Fig. S6. Cryo-EM observation of CAP-Gly1–144 and tubulin copolymerization at t = 300 s. Compared with the normal tubulin polymerization (*Upper Right*), formation of significantly more sheets and curved oligomers is visible in the background. (*Lower*) Zoomed-in views of the sheet-like structures. Pink dotted lines in the upper row are guidelines for the observed densities as shown unperturbed in the lower row. The arrangements of the curved oligomers to sheet-like polymers are shown in the presence of CAP-Gly1–144 (*Left*) in comparison with tubulin alone (*Right*).

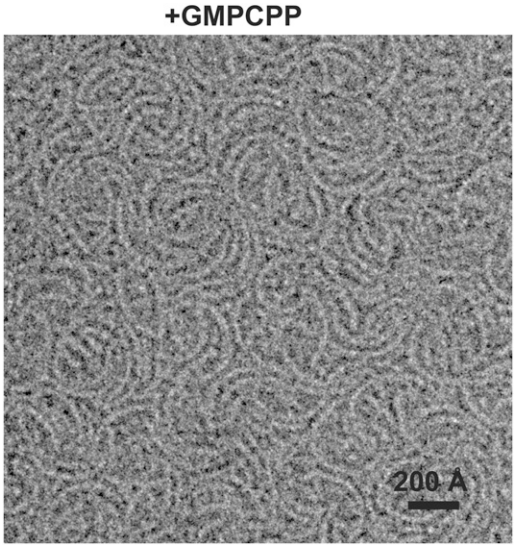

Fig. S7. Tubulin oligomers in the presence of p150(1–144) and GMPCPP, showing curved tubulin oligomers as well.

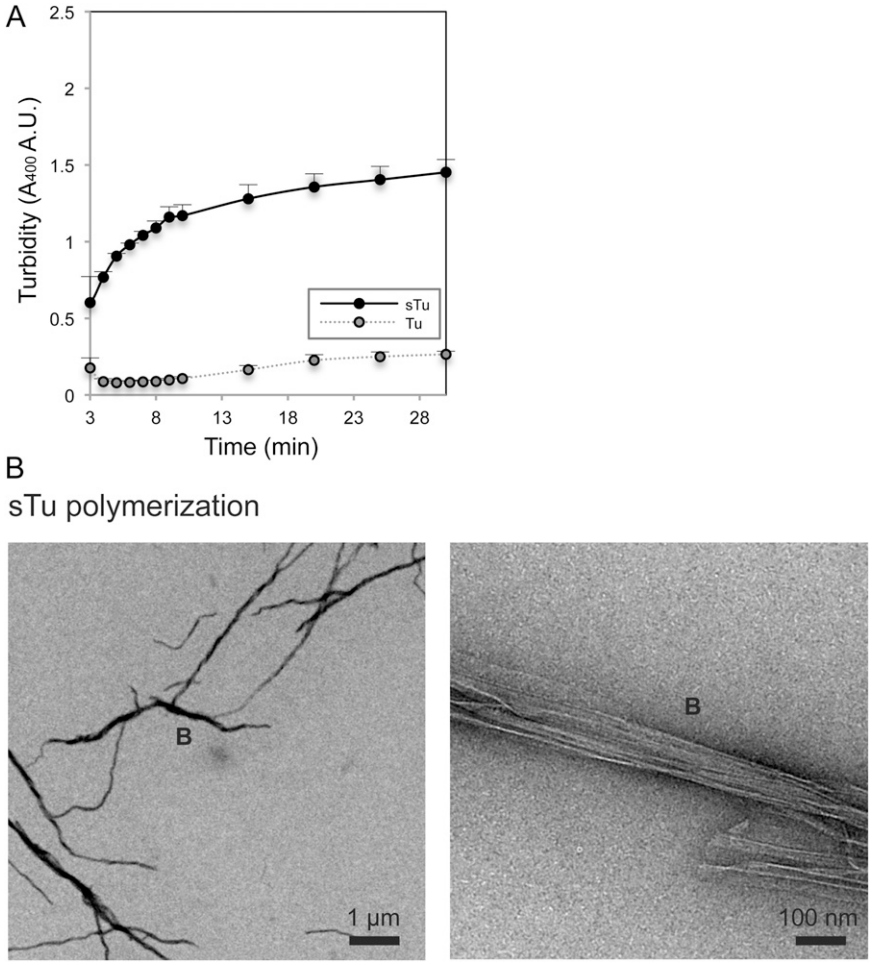

Fig. S8. Polymerization profile of subtilisin-treated tubulins (sTu). (*A*) sTu polymerization profile. Increase of the scattering is observed. (*B*) The polymerized products show mostly bundles or open sheets laterally associated with each other.

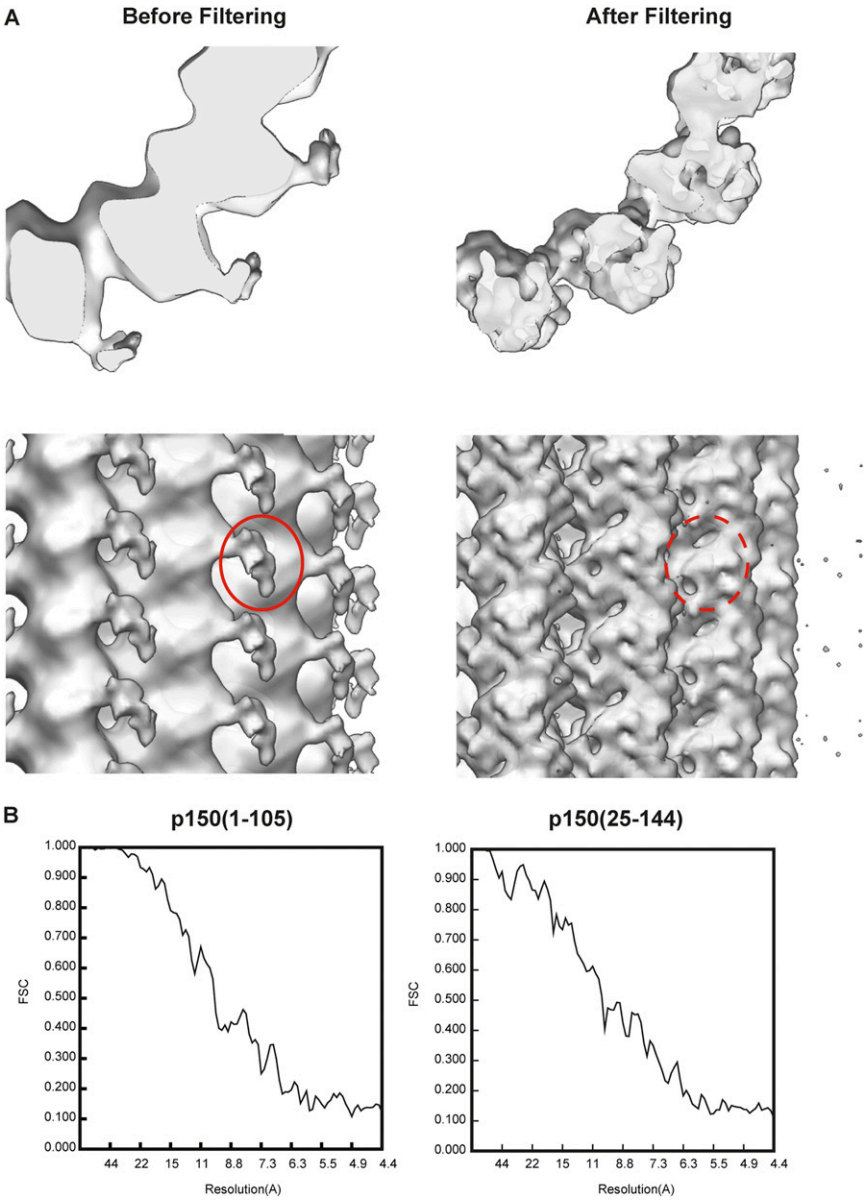

Fig. S9. (*A*) A 3D reconstructions of the microtubule-p150(1–105) complex. Due to the flexible binding of p150(1–105) to the microtubule, amplitude-corrected reconstructions (After Filtering) no longer show the densities corresponding to the CAP-Gly (red dotted circle on the side view) whereas the amplitude-uncorrected reconstructions clearly show the CAP-Gly decorations (red solid circle). (*B*) Fourier shell correlations (FSCs) of the reconstructions of p150(1–105)-microtubules (*Left*) and p150(25–144)-microtubules (*Right*).